6th International Conference on Advances in Experimental Structural Engineering
11th International Workshop on Advanced Smart Materials and Smart Structures Technology
August 1-2, 2015, University of Illinois, Urbana-Champaign, United States

On the study of the influences of temperature and axial load to the impedance-based structural health monitoring system

Xuan Zhu[1], Francesco Lanza di Scalea[2], Mahmood Fateh[3]

1 *Graduate student researcher, Dept Structural Engineering, University of California, San Diego, USA. E-mail: xuz009@ucsd.edu*
2 *Professor, Dept Structural Engineering, University of California, San Diego, USA. E-mail: flanza@ucsd.edu*
3 *Office of Research and Development, Federal Railroad Administration, Washington, DC, USA E-mail: mahmood.fateh@dot.gov*

ABSTRACT
Structural Health Monitoring (SHM) has attracted researchers focus in the last two decades to handle the aging infrastructure systems all over the world. As one of the potential solutions, the Electro-Mechanical Impedance (EMI) method was introduced in the early 1990s and has a great number of potential applications in the SHM of civil, mechanical and aerospace industries. This paper presents current investigations on the feasibility of using an EMI-based SHM technique to monitor the thermal stresses in the Continuous Welded Rail (CWR). This work is important to prevent train accidents due to either rail buckling (in hot weather) or rail breakage (in cold weather). The objective of this research is to develop a model parameter-based temperature compensation framework to eliminate the influence of temperature variations on the EM signatures when both the temperature and thermal load influent the EMI measurements. A comparative study is conducted between the proposed temperature compensation algorithm and the traditional method on previous experimental datasets. The final results illustrate that the proposed algorithm is capable to eliminate the temperature effect and highlight the ones from thermal load.

KEYWORDS: *SHM, EMI, temperature effect, piezoelectricity*

1. INTRODUCTION

Electro-mechanical impedance method, introduced in the early 1990s [1-3], is an active sensing approach which characterizes the point-wise mechanical impedance of the host structure by using the electrical impedance of a bonded or embedded PZT wafer [4]. The electrical admittance, directly measureable by impedance analyzer, LCR meter or any embedded impedance measurement system, is a function of the stiffness, mass, and damping of the host structure [5] the length, width, thickness, orientation, and mass of the PZT, as well as the adhesive utilized to bond the PZT to the structure [6]. Therefore, assuming the physical properties of the adhesive and PZT remain constant, the presence of deviation from the baseline condition, such as structural damage or stress distribution changes, can be characterized by the variations in the admittance.

EMI has attracted attentions for in-situ structural integrity assessments. For the modeling investigations, Liang et al. [1,2] developed the first coupled electro-mechanical analysis of piezoelectric ceramic actuators integrated in a spring-mass-damper system to bridge the structural mechanical impedance and the PZT's electrical admittance. The authors then applied dynamic analysis on both the actuator and the structure to determine the structural impedance; Zhou et al. [3] developed a dynamic model of distributed PZT actuators coupled with two-dimensional structure, and applied a thermal stress analysis on the PZT elements with a one-dimensional heat conduction model; Yang et al. proposed a novel simplified two-dimensional interactions of the PZT with the host structure with one single complex terms based on the concept of effective impedance [7]. Giugiutiu and Zagrai developed the coupling model based on longitudinal vibration combined with piezoelectricity [4,8]. They computed the pointwise dynamic stiffness including the structural dynamics .Ong et al. studied the axial loading effect on EMI method by adding the axial effect into the Euler-Bernoulli beam vibration [9].

On the experimental studies, Giurgiutiu and Rogers reported the ability of EMI to be implemented as a SHM method for detection of the onset of delimitations, cracks, and disbonds in composite plates [10]. Park and Inman illustrated the potentials of applying EMI on the SHM for composite reinforce structures damage detection and loosened bolt detection and summarized the signal processing techniques for impedance-based

SHM [5]. Park et al. proposed EMI as a sensor self-diagnostics method and applied the temperature effects-free damage detection techniques based on the maximum cross-correlation coefficient [11]. Annamdas et al. induced a comprehensive experimental study on the influence of loading on the impedance-based method [12]. Yang et al. measured the propagation of damage in a plate with the EMI technique [13]. Annamdas et al., Yang et al., and Lim et al. all reported the results of their experiments to measure the loading of test specimens [12-15].

Through these studies, the EMI method shows a good potential to identify the structural condition variations, mostly caused by damage, via changes in the resonance frequencies of the structure in a variety of structural configurations. The specific application of interest to the present study is the measurement of thermal loads in Continuous-Welded Rail (CWR), which is still an unresolved problem in railroad maintenance today. Thermal stresses develop due to constrained thermal expansion of the welded track. In particular, tensile stresses develop under cold weather, whereas compressive stresses develop under warm weather. Excessive tensile stresses can develop fractures, and excessive compressive stresses can induce buckling. Both cases are high-priority safety hazards in railroad transportation. Buckling in hot weather (the sunkink) had been responsible for over 57M dollars lost from 2006-2011 and caused 3.4% of derailments and 12.7 cars derailed per derailments from 2000-2010 [16]. The well-known formula that governs the thermal loads in CWR is [17].

$$P=\alpha\, E\, A\, (T-NT) \tag{1.1}$$

, where P is the thermal load, α is the coefficient of thermal expansion of steel, E is the Young's Modulus of steel, A is the rail cross-sectional area, T is the rail temperature, and NT is the so-called 'rail Neutral Temperature'. Knowledge of the rail Neutral Temperature, which corresponds to the rail temperature when the rail has zero thermal stress, is of outmost importance to rail engineers. This paper explores the EMI method as a possible solution to measure the in-situ thermal stresses in rails and estimate the rail neutral temperature. In present study, to quantify the variations of the EM signatures, the index of Root Mean Square Deviation (RMSD) [5], as a measure of the residual difference from a baseline measurement, is investigated:

$$\mathrm{RMSD}(\%) = \sqrt{\frac{\sum_{i=1}^{N}(y_i-x_i)^2}{\sum_{i=1}^{N} x_i^2}} \times 100 \tag{1.2}$$

, where $\boldsymbol{y_i}$ is the baseline admittance value and $\boldsymbol{x_i}$ is the measurement admittance.

This paper is organized as follow: section 2 reviews the concepts and the analytical model of EMI method; section 3 describes a proposed temperature compensation framework and conducts a comparative study on previous experimental datasets; the paper concludes in section 4.

2. REVIEW ON EMI METHOD AND THE ANALYTICAL MODEL

The structural impedance and the electrical admittance of the bonded PZT patch were bridged by the one-dimensional Electro-Mechanical modeling of a piezoelectric actuator-driven system [1-4]. Consider a PZT wafer bonded on the structure, the PZT-structural dynamic interaction is determined by coupling the constitutive relation of the PZT and the structure with their equations of motion. If only considering the in-plane strain induced by the constitutive relations of the PZT (T, E type) are:

$$\begin{cases} S_1 = s_{11}^E T_1 + d_{31} E_3 \\ D_3 = \varepsilon_{33}^T E_3 + d_{31} T_1 \end{cases} \tag{2.1}$$

, where S_1 is the strain, T_1 is the stress, D_3 is the electric displacement, s_{11}^E is the mechanical compliance at zero field, ε_{33}^T is the dielectric constant at zero stress, d_{31} is the piezoelectric parameter. By introducing the quasi-static stiffness of the PZT patch, considering the force equilibrium at the boundaries and Newton's law of motion, the admittance (inverse of impedance) can be found as [4,8]:

$$Y = i\omega C\left[1 - K_{31}^2\left(1 - \frac{1}{\varphi\cot(\varphi)+r}\right)\right] \tag{2.2}$$

, where $C = \varepsilon_{33}^T \frac{b_a l_a}{t_a}, K_{31}^2 = \frac{d_{31}^2}{s_{11}^E \varepsilon_{33}^T}, \varphi = \frac{1}{2}\gamma l_a, r = \frac{K_{str}}{K_{PZT}}, \gamma = \frac{\omega}{c}, c^2 = \frac{1}{s_{11}^E \rho_a}$, ρ_a is the density of the PZT, b_a, l_a, h_a are the geometry of the PZT actuator, ω is the excitation frequency, d_{31} is the PZT piezoelectric constant, ε_{33}^T is the PZT complex dielectric constant at zero stress, s_{11}^E is the PZT complex compliance

modulus at zero electric field, K_{str} and K_{PZT} are the structural stiffness of PZT and structure, respectively. Eq. 2.2 clearly shows that the electrical admittance (or impedance) of the PZT is directly related to the stiffness of the substructure. Assuming that the properties of the PZT do not change during the measurement period, variations in the electrical impedance signatures are related to variations of the structural stiffness.

Given the electromechanical admittance model in Eq. 2.2, the structural stiffness K_{str} of an Euler-Bernoulli beam has been derived via eigenfunction expansion method by [4,9,14]. In this study, in order to investigate the variations lead by temperature and axial loading, this derivation will be briefly summarized. For temperature-sensitive parameters in the model, a linear dependence of each property on temperature is assumed: $X(T) = X(T_0) + \frac{\partial X(T)}{\partial T}\Delta T$, where X represents the parameters include mechanical and piezoelectric properties, T is the generic temperature, T_0 is the ambient temperature (assumed 20℃), and $\frac{\partial X(T)}{\partial T}$ is the sensitivity to temperature [18]. Furthermore, by introducing the actuated shear stress model into the spatial distribution of excitation, this work enables the potential of introducing the shear-lag effect modeling from the actuation aspect. The derivations in details can be found in previous work [19].

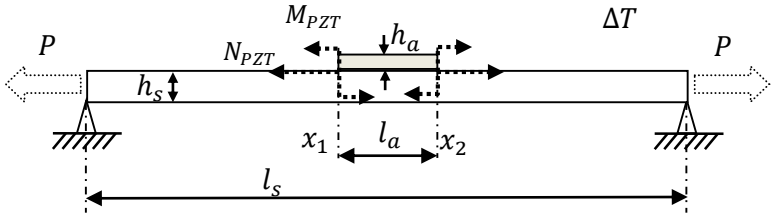

Figure 2.1 A simply supported beam subjected to axial loading
and temperature variations and the external loads from PZT patch.

For mathematical simplification, only the model of the simply supported boundary condition was developed explicitly to predict the admittance behaviors when the variations of temperature/axial loading present as shown in Fig. 2.1. The input distribution function is represented by Dirac Delta function: the axial force $N_{PZT}(x) = F_{PZT}[-\delta(x-x_1) + \delta(x-x_2)]$, the bending moment $M_{PZT}(x) = \frac{F_{PZT}(h_s+h_a)}{2}[\delta(x-x_1) - \delta(x-x_2)]$, where F_{PZT} is the force excited from PZT, h_s is the thickness of the structure, h_a is the thickness of the actuator, x_1 and x_2 are the positions of two ends of PZT, δ is the Dirac Delta function, and $F_{PZT}(h_s + h_a)$ is the magnitude of pure bending moment provided by PZT.

First, the longitudinal vibration with distributed force loading on the simply support Euler-Bernoulli Beam will be computed. Assuming the cross section is constant and the axial force is distributed evenly through x axis, the governing equation can be written as [20]:

$$\mathrm{EA}\frac{\partial^2 \mathrm{u(x,t)}}{\partial \mathrm{x}^2} + \mathrm{N(x,t)} = \rho \mathrm{A}\frac{\partial^2 \mathrm{u(x,t)}}{\partial \mathrm{t}^2} \tag{2.3}$$

, where *E* is the Young's modulus of the material, *A* is area of cross section, *u* is the longitudinal displacement, *N* is the external distributed force, ρ is the density of the material. With the harmonic excitation, in order to obtain the steady-state solution, separation of variables is applied: $\mathrm{u(x,t)} = \mathrm{u(x)e^{i\omega t}}$. With the pin-pin boundary condition, the eigenfunction was solved as $\mathrm{u(x)} = \mathrm{Bsin}\left(\frac{\mathrm{n\pi}}{\mathrm{l_s}}\mathrm{x}\right)$. By using the orthogonality of the eignmodes and integration by parts to compute the participation coefficient, the displacement induced by the longitudinal vibration could be represented as:

$$u(x,t) = e^{i\omega t}\frac{2F_{PZT}}{\mathrm{l_s}}\sum_{n=0}^{\infty}\frac{\left[-\sin\left(\frac{\mathrm{n\pi}}{\mathrm{l_s}}\mathrm{x_1}\right)+\sin\left(\frac{\mathrm{n\pi}}{\mathrm{l_s}}\mathrm{x_2}\right)\right]}{\mathrm{EA}\left(\frac{\mathrm{n\pi}}{\mathrm{l_s}}\right)^2 - \rho\mathrm{A}\omega^2}\sin\left(\frac{n\pi}{l_s}x\right) \tag{2.4}$$

To compute the displacement induced by the transverse vibration of a simply support Euler-Bernoulli Beam subjected to axial loading *P*, by assuming the cross section is consistent and the axial force is distributed evenly through x axis, the governing equation can be written as [20]:

$$\mathrm{EI}\frac{\partial^4 \mathrm{w(x,t)}}{\partial \mathrm{x}^4} + \rho\mathrm{A}\frac{\partial^2 \mathrm{w(x,t)}}{\partial \mathrm{t}^2} - \mathrm{P}\frac{\partial^2 \mathrm{w(x,t)}}{\partial \mathrm{x}^2} = -\frac{\partial \mathrm{M(x,t)}}{\partial \mathrm{x}} \tag{2.5}$$

, where w is the transverse deflection, E is the Young's modulus of the material, A is area of cross section, u is the longitudinal displacement, I is the moment of inertia of the beam, M is the external distributed moment, ρ is the density of the material, P is the applied axial load. Applying the same technique as previous step, the deflection can be represented as:

$$w(x,t) = e^{i\omega t}\frac{\pi F_{PZT}(h_s+h_a)}{l_s^2}\sum_{n=1}^{\infty} n\frac{\left[\cos\left(\frac{n\pi}{l_s}x_1\right)-\cos\left(\frac{n\pi}{l_s}x_2\right)\right]}{EI\left(\frac{n\pi}{l_s}\right)^4-\rho A\omega^2+P\left(\frac{n\pi}{l_s}\right)^2}\sin\left(\frac{n\pi}{l_s}x\right) \tag{2.6}$$

The deformation of the PZT can be computed as in [4]:

$$u_{PZT}(x,t) = \mathrm{u}(x,t)|x_1 - \mathrm{u}(x,t)|x_2 - \left(\frac{h_s}{2}\right)[w'(x,t)|x_1 - w'(x,t)|x_2] \tag{2.7}$$

Thus, the point-wise structural stiffness can be computed as:

$$\mathrm{K_{str}} = \frac{\mathrm{F_{PZT}}}{\mathrm{u_{PZT}}} = \left(\left\{\frac{2}{\mathrm{l_s}}\sum_{n=0}^{\infty}\mathrm{X_n} + \frac{\pi^2 \mathrm{h_s(h_s+h_a)}}{\mathrm{l_s^3}}\sum_{\mathrm{n=0}}^{\infty}\mathrm{Y_n}\right\}\right)^{-1} \tag{2.8}$$

, where $X_n = \frac{\left[sin\left(\frac{n\pi}{l_s}x_1\right)-sin\left(\frac{n\pi}{l_s}x_2\right)\right]^2}{EA\left(\frac{n\pi}{l_s}\right)^2-\rho A\omega^2}$, $Y_n = n^2\frac{\left[cos\left(\frac{n\pi}{l_s}x_1\right)-cos\left(\frac{n\pi}{l_s}x_2\right)\right]^2}{EI\left(\frac{n\pi}{l_s}\right)^4-\rho A\omega^2+P\left(\frac{n\pi}{l_s}\right)^2}$, l_s and h_s are the length and the thickness of the beam, h_a is the thickness of PZT patch, E is the Young's modulus of the beam, ρ is the density of the beam, A is the area of cross section of the beam, I is the moment of inertia of the beam, P is the applied axial load on the structure, x_1 and x_2 are the two ends of the PZT patch and ω is the angular frequency. Given the Eq. 2.8, the structural stiffness can be coupled with the EMI model from Eq. 2.2, which includes the effects of temperature and axial loading on the underlying structure. The analytical model to predict the EM signatures under the influences of the axial load and temperature has been verified in previous study [19].

3. THE TEMPERATURE COMPENSATION ALGORITHM BASED ON MODEL PARAMETERS

According to previous study [19], the effect of temperature potentially dominate the variations of the EM signature which could either result in a false alarm for defect detection or false negative with burying any noticeable changes caused by factors other than temperature. Both the axial load and temperature effects were studied by comparing the analytical and experimental results. And the ranges in experiments were configured as the typical load and temperature levels for on-service CWRs around the neutral temperature. It had been shown that the signature variations at selected frequency bands led from axial load, ranged from -80 MPa to 54 MPa, can reach to 13% deviation from the signatures at zero stress state, while a 90% deviation from the baseline can be observed for the temperatures ranged from ambient to 75℃. A compensation algorithm is desired to eliminate the temperature influence on the EM signature and there are currently available methods to determine the effective frequency shift (EFS) [11,21], which utilize criteria such as maximum cross correlation or minimum RMSD to identify the frequency shift led by temperature variation and inversely shift the signatures back.

In the present study, a novel temperature compensation algorithm based on model parameters is proposed. As shown in Fig. 3.1, the Eq. 2.2 can be rewritten into two parts: the first two terms are the passive signatures, which only depend on the excitation frequency, piezoelectric and dielectric properties of PZT patch; the third term composes by the temperature-sensitive properties from PZT and the active signature part which is mainly related to the structural dynamic properties. Therefore, the active signature would be an excellent indicator for variations of structural properties, which is also immune from the temperature-sensitive properties of the PZT patch. Based on this concept, a novel temperature compensation framework for EMI method is proposed as shown in Fig. 3.2: the first step is to record the baseline Y_{base} at ambient temperature T_0 and take the measurement Y_{meas} at temperature T; to extract the active signature Y_{Act}, the passive signature is subtracted from the measurements, then normalized by the excitation frequency and the temperature-sensitive parameters, which are estimated by the linear dependence on temperature; the active signatures are fed into the minimum RMSD algorithm [21] to determine the frequency and the magnitude shifts (φ_f and φ_m) between the active signatures from measurement and baseline; Y_{Act} of measurement would be inversely shifted towards the Y_{Act}

of the baseline to compensate the variations led from previous operation of active signatures extraction, which finally results in the temperature-compensated active signature $Y_{Act-Tcomp}$.
The performance of the proposed framework would be evaluated with the comparison to the minimum RMSD temperature compensation strategy, applied on two datasets from previous study [19]. The experimental setup is shown in Fig. 3.3(a-b), and the temperature and thermal load ranges are shown in Fig. 3.3(c-d). In test 3, a simply supported 136RE rail track is heated by the heating element from 25℃ up to 70℃, and ideally no thermal stress is built up during the test. In test 4, a constrained 136RE rail track is heated by the heating element at the UCSD/FRA rail buckling testbed. The same temperature range is covered and the thermal stresses are ranged from 30 MPa to -60 MPa. The measurements at the ambient temperature are set as baselines in both tests respectively.

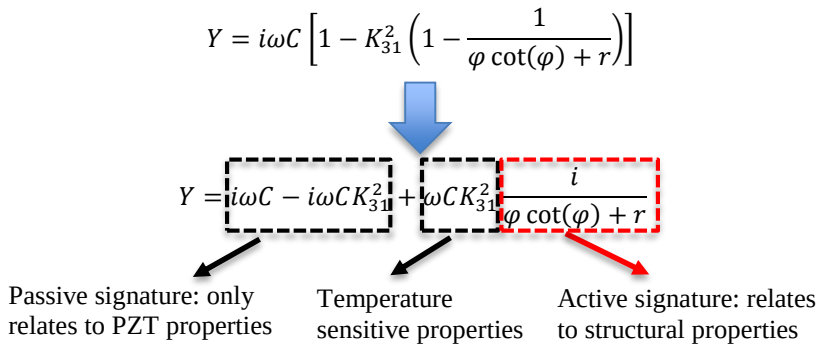

Figure 3.1 The discoveries when Eq. 2.2 is rewritten

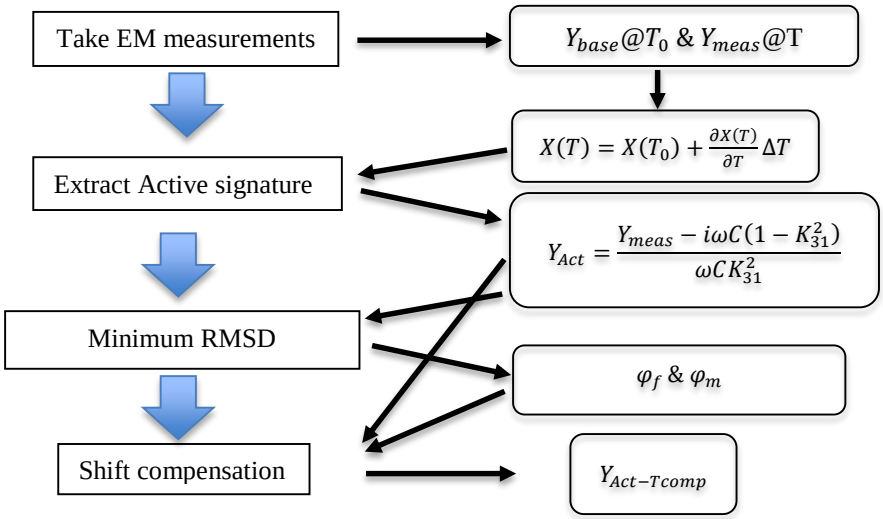

Figure 3.2 The proposed temperature compensation framework

The EM signatures from test 3 and test 4 are shown in Fig. 3.4. In test 3, only the temperature variations are introduced. For the conductance shown in Fig. 3.4(a), the magnitude increases and the main resonance peak shifts towards lower frequencies as the temperature raises; for the susceptance shown in Fig. 3.4(b), the slope of the signature increases as with temperatures raises. In test 4, both the temperature and thermal stress variations are introduced. For the conductance and susceptance shown in Fig. 3.4(c-d), similar behavior is observed in the real and imaginary parts as test 3, mainly resulted from the temperature variations, where the influence of thermal stress is entirely buried. At this stage, it becomes very difficult to differentiate the effect from temperature and the one from thermal load, since they present simultaneously.

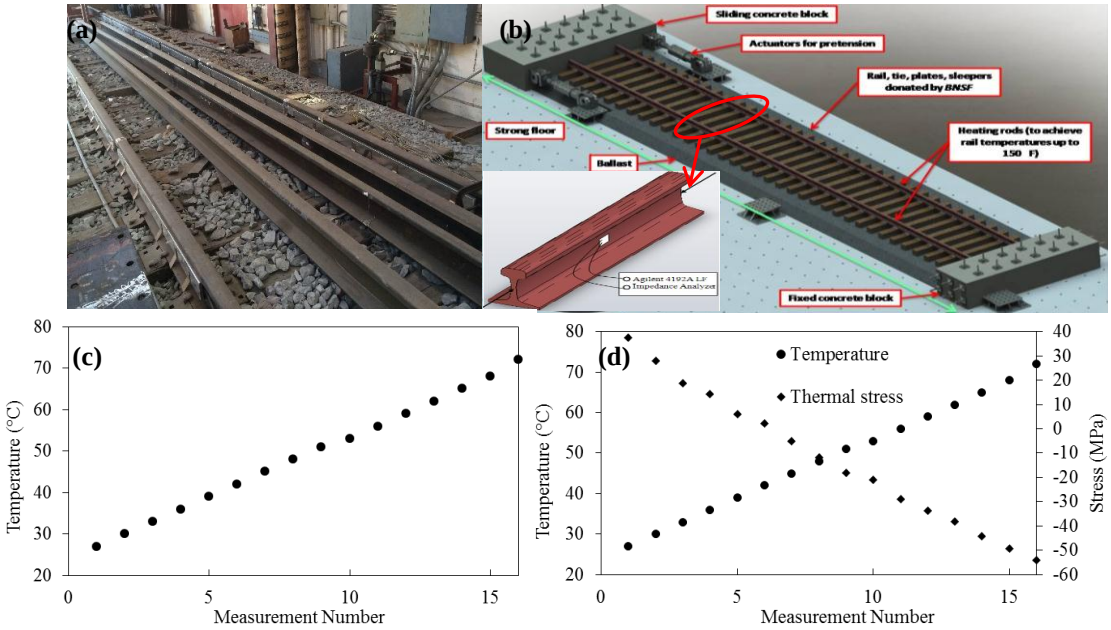

Figure 3.3 (a) experimental setup for test 3; (b) experimental setup for test 4;
(c) the temperature variation in test 3; (d) the temperature and thermal stress variation in test 4

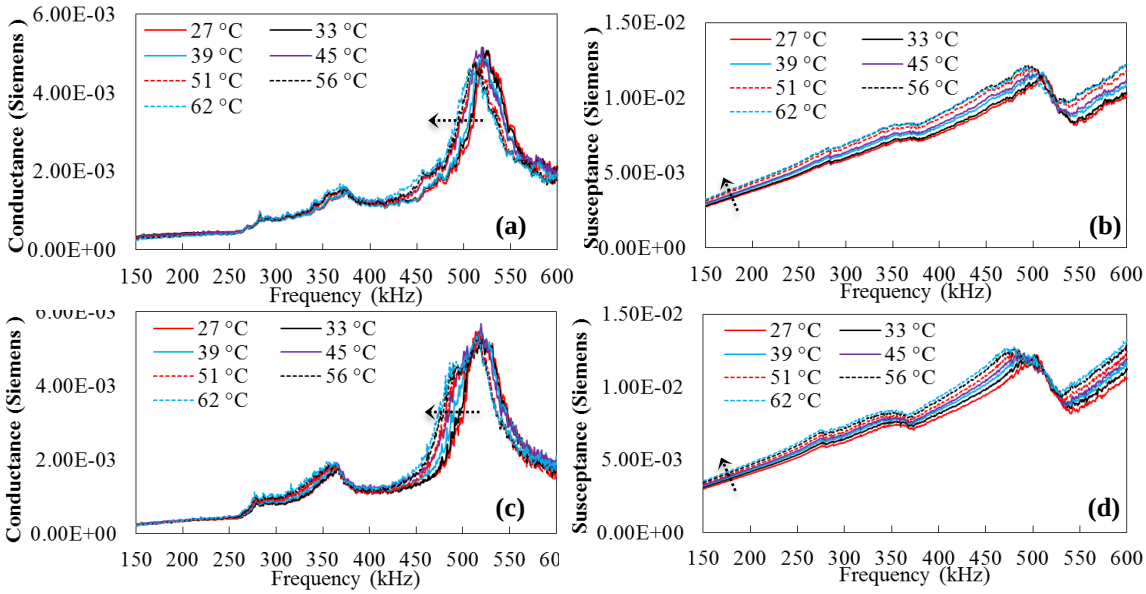

Figure 3.4 Typical EM signatures from Test 3: (a) Conductance; (b) Susceptance
and from Test 4: (c) Conductance; (d) Susceptance

The RMSD values are extracted from the original susceptance measurements for two frequency bands from test 3 and 4, as shown in Fig.3.5 (a-b). The red circles stand for the results from test 3 and the black dots represent the ones from test 4. As the temperature increases from 25℃ to 70℃, the RMSD values from test 3 and 4 reach the similar level of deviation (17-20%) from the ambient baseline for both frequency band 1 and 2. At this stage, there is no visible difference between the two tests. Secondly, the minimum RMSD method is implemented on the original susceptance of two frequency bands from test 3 and 4, as shown in Fig. 3.5 (c-d). The RMSD values of the minimum RMSD results are lowered within 2% of the deviation from the baseline, in which this method significantly suppresses any deviations from the baseline. The variations are over-compensated and no obvious differentiation is observed between test 3 and 4, in which the purpose to highlight the effect of thermal stress from those of temperature is not satisfied. Thirdly, after applying the proposed temperature compensation framework, the RMSD values of frequency band 1 and 2 are shown in Fig.3.5 (e-f) for the free thermal expansion case (test 3) and constrained thermal expansion case (test 4). The RMSD values for test 3, as a

measure of the deviation from the measurement at ambient temperature, is lowered within 7% after applied the proposed method. On the other hand, the values for test 4 reach 37% in frequency band 1, indicating its sensitivity to the thermal stress. Similar performance can be observed for the frequency band 2 in Fig. 3.5(f). The study on multiply frequency bands has been conducted and the similar performances are observed. At this point, it concludes that the proposed algorithm is capable to eliminate the temperature effect on the PZT patch by normalizing the signatures with the temperature-sensitive parameters on piezoelectricity and highlight the thermal stress influence on the structural dynamic properties via the extraction of the active signatures. A further study is needed to calibrate the RMSD values after the proposed algorithm with the thermal stress, in order to determine the rail neutral temperature. The same strategy can be easily implemented on the applications of EMI-based defect detection with temperature variations.

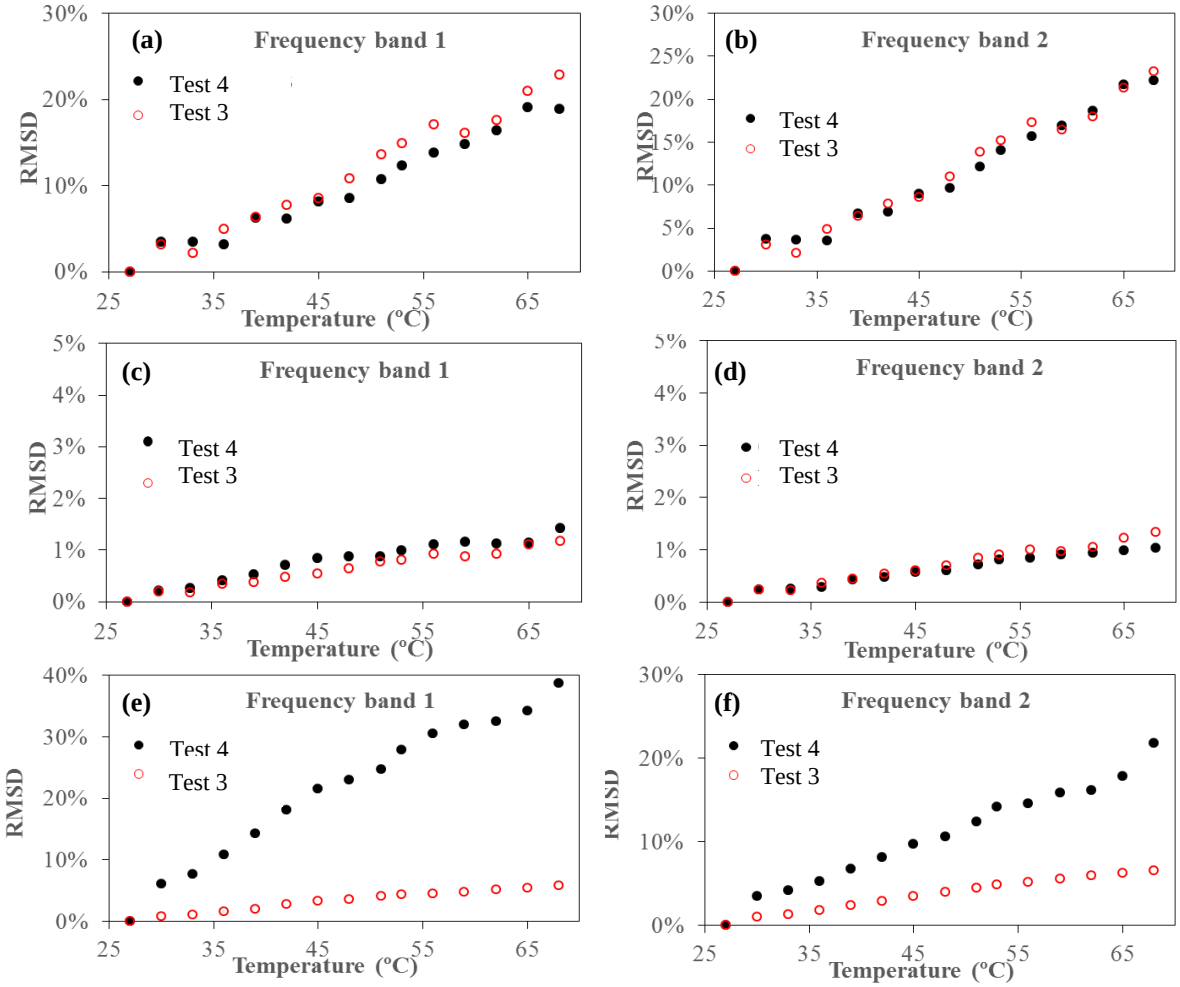

Figure 3.5 The RMSD values from frequency band 1 based on (a) original admittance (c) susceptance after EFS (e) susceptance after proposed framework; the RMSD values from frequency band 2 based on (b) original admittance (d) susceptance after EFS (f) susceptance after proposed framework.

4. CONCLUSION

This study proposes an innovated model parameter-based temperature compensation framework for EMI method, particularly its application in CWRs. The analytical model to predict the EM signatures under temperature and axial load effects is first reviewed to understand the inherent electro-mechanical coupling mechanism of the EMI method and the behaviors of EM signatures under the influences from axial load and temperature. Taking advantage of being able to accurately predict the EM signatures under temperature variations, the passive signatures are first eliminated from the measurements, and the results are normalized by the temperature-sensitive model parameters on piezoelectricity. The proposed framework is implemented on two sets of experiments: a free-to-expand 136RE rail track is heated in test 3; a constrained 136RE rail track is heated in test 4. While neither the RMSD values of the raw measurements or the ones of minimum

RMSD-compensated signatures are able to differentiate the temperature-only case (test 3) and the thermal-stress case (test 4), the proposed framework successfully suppresses the temperature influence and highlights the thermal stress effect on the EM signatures. A further study on calibrating the active signature with the thermal load is needed to determine the in-situ thermal stress in CWR.

ACKNOWLEDGMENTS

This project is supported by the U.S. Federal Railroad Administration. The Program Manager is Mahmood Fateh from the FRA Office of Research and Development. Special recognition is extended to the Burlington Northern Santa Fe (BNSF) railway for providing in-kind support for the rail tracks and the exchange of technical information.

REFERENCE

1. Liang, C., Sun, F. P., Rogers, C. A. (1994). Coupled electro-mechanical analysis of adaptive material systems determination of the actuator power consumption and system energy transfer. *J. Intell. Mater. Syst. Struct.*, **5**, 12-20.
2. Liang, C., Sun, F. P. and Rogers, C. A. (1996). Electro-mechanical impedance modeling of active material systems. *Smart Mater. Struct.*, **5**, 171–186.
3. Zhou, S., Liang, C. and Rogers, C. A. (1996).An Impedance-Based System Modeling Approach for Induced Strain Actuator-Driven Structures. *Journal of Vibration and Acoustics*, **3(118)**, 323-331.
4. Giurgiutiu, V., Zagrai, A.N. (2000). Characterization of Piezoelectric Wafer Active Sensors. *J. Intell. Mater. Syst. Struct.*, **11**, 959 –976.
5. Park, G., Inman, D.J. (2007). Structural health monitoring using piezoelectric impedance measurements. *Phil. Trans. R. Soc. A*, **365**, 373–392.
6. Bhalla, S., Soh, C. K. (2004). Electromechanical Impedance Modeling for Adhesively Bonded Piezo-Transducers. *J. Intell. Mater. Syst. Struct.*, **15**, 955.
7. Yang, Y. Xu, J., Soh, C. K. (2005). Generic Impedance-Based Model for Structure-Piezoceramic Interacting System. *Journal of Aerospace Engineering*, **18**.
8. Giurgiutiu, V., Zagrai, A.N. (2002). Embedded Self-Sensing Piezoelectric Active Sensors for On-line Structural Identification. *Journal of Vibration and Acoustics*, **124**, 116-125.
9. Ong, C.W., Yang, Y., Naidu, A.S.K., Lu, Y., Soh, C. K. (2002). Application of the electro-mechanical impedance method for the identification of in-situ stress in structures. *Proceedings of SPIE*, **4935**.
10. Giurgiutiu, V., Rogers, C.A. (1998). Recent advancements in the electromechanical (E/M) impedance method for structural health monitoring and NDE. *Proceedings of SPIE*, 536–547.
11. Park, S., Lee, J., Yun, C., Inman, D. J. (2008). Electro-Mechanical Impedance-based Wireless Structural Health Monitoring Using PCA-Data Compression and k-means Clustering Algorithms. *J. Intell. Mater. Syst. Struct.*, **19**.
12. Annamdas, V.G.M., Yang, Y., Soh, C.K. (2007). Influence of loading on the electromechanical admittance of piezoceramic transducers. *Smart Materials and Structures*, **16**, 1888–1897.
13. Yang, Y., Liu, H., Annamdas, V.G.M., Soh, C.K. (2009). Monitoring damage propagation using PZT impedance transducers. *Smart Materials and Structures*, **18**, 045003.
14. Annamdas, V.G.M., Rizzo, P. (2009). Influence of the excitation frequency in the electromechanical impedance method for SHM applications. *Proceedings of SPIE*, 72930V–72930V–11.
15. Lim, Y.Y., Soh, C.K. (2012). Effect of Varying Axial Load Under Fixed Boundary Condition on Admittance Signatures of Electromechanical Impedance Technique. *J. Intell. Mater. Syst. Struct.*, **23**, 815–826.
16. Liu, X., Rapik Saat, M., Barkan, C. P. L. (2012). Analysis of causes of major train derailment and their effect on accident rates. *Transportation Research Record: Journal of the Transportation research board*, 2289.
17. Kerr, A. (1978). Analysis of thermal track buckling in the lateral plane. *Acta Mechanica*, **30**, 17–50.
18 Lanza di Scalea, F., Salamone, S. (2008). Temperature effects in ultrasonic Lamb wave structural health monitoring systems. *J. Acoust. Soc. Am.*, **1**, 124.
19 Zhu, X., Lanza di Scalea, F., Fateh, M.(2014). Temperature and axial stress effects in electro-mechanical impedance method-based structural health monitoring. *SPIE Proceedings*, **9064**.
20 Rao, S. S.(2003). Mechanical Vibrations, Prentice Hall, Lebanon, Indiana.
21 Park, G., Kabeya, K., Cudney, H. H., Inman, D. J. (1999). Impedance Based Structural Health Monitoring for temperature Varying Applications. *JSME International Journal*, **2**, 42.